Evidence of sub-MeV EMIC-driven trapped electron flux dropouts from GPS observations

A. T. Hendry[1], C. J. Rodger[1], M. A. Clilverd[2], S. K. Morley[3]

[1]Department of Physics, University of Otago, Dunedin, New Zealand
[2]British Antarctic Survey (UKRI-NERC), Cambridge, UK
[3]Space Science and Applications, Los Alamos National Laboratory, Los Alamos, New Mexico, USA

Key Points:

- Electromagnetic ion cyclotron waves can cause measurable depletion of sub-MeV trapped radiation belt electrons.
- Primarily sub-MeV loss observations and primarily relativistic trapped-flux depletions are not in direct contradiction.
- We present statistical evidence of ultra-relativistic trapped electron flux depletions, confirming existing published case study results.

Corresponding author: Aaron T. Hendry, aaron.hendry@otago.ac.nz

Abstract

For many years, it was believed that resonant interactions between electromagnetic ion cyclotron (EMIC) waves and radiation belt electrons were restricted to electron energies $> 1 - 2$ MeV. In recent years, however, a growing body of experimental evidence has shown that EMIC waves can cause the scattering loss of electrons down to sub-MeV energies. Using measurements of trapped electron flux from the GPS satellite constellation, we investigate the ability of EMIC waves to cause significant depletions of radiation belt electron populations between $4 \leq L^* \leq 5$. For the first time, we present statistical evidence demonstrating global decreases in sub-MeV trapped electron flux in response to EMIC wave activity. Although we find that electron losses extend down to sub-MeV energies, we also show strong statistical support for the ability of EMIC waves to preferentially cause substantial depletions of ultra-relativistic electrons in the radiation belts.

Plain Language Summary

Electromagnetic ion cyclotron (EMIC) waves are a type of extremely low frequency electromagnetic wave commonly found within the Earth's radiation belts. Although it has long been known that these waves are capable of driving energetic electrons out of the belts and into the Earth's atmosphere, the energy limits of this interaction are still a matter of considerable debate. In this study, we combine many years of data from electron detectors carried by multiple GPS satellites to statistically investigate the effects of EMIC waves on radiation belt electron populations. We show that these waves are capable of causing significant decreases in electron populations at energies much lower than has previously been considered possible. This result has important ramifications not only for our models of how radiation belt electron populations change over time, but also for our understanding of how EMIC waves are linked to chemical changes in the Earth's atmosphere.

1 Introduction

In recent years there has been considerable scientific debate surrounding electromagnetic ion cyclotron (EMIC) waves and their ability to interact with radiation belt electrons. The fact that this interaction can take place is uncontroversial, but the energy range of the interaction has been the cause of significant disagreement. To a certain extent, this is the result of uncertainty as to the actual physical interaction(s) behind this process (e.g. Meredith et al., 2003; Loto'aniu et al., 2006; L. Chen et al., 2011; Omura & Zhao, 2013; L. Chen et al., 2016; Denton et al., 2019), however discrepancies between individual experimental results have also been cause for some concern (e.g. Usanova et al., 2014; Shprits et al., 2016; Hendry et al., 2017; Capannolo et al., 2019). Accurate knowledge of the energy limits of EMIC-electron interactions is important not only to improve our understanding of radiation belt dynamics, but also to understand the impact of EMIC-driven electron precipitation (EMIC-EP) on the Earth's atmosphere. Energetic electron precipitation (EEP) has been recognised as a significant driver of atmospheric climate variability (e.g. Matthes et al., 2017), with EMIC acknowledged as a potentially important source of such EEP (Hendry et al., 2021). However, without proper understanding of the loss processes involved in driving this EEP, and the resultant characterisation of its energy range, it is difficult to properly account for it in models.

For many years, the generally accepted lower energy limit of EMIC-electron interactions has been on the order of 1–2 MeV, based on statistical studies such as (Meredith et al., 2003). This limit has been supported by in-situ experimental observations of trapped electron flux (e.g. Usanova et al., 2014; Shprits et al., 2016), which have suggested that EMIC-driven electron flux dropouts are limited to relativistic or ultra-relativistic energies. The science on this issue is far from settled, however. Indeed, this relativistic limit is not actually a *theoretical* limit, but rather a limit based on observations. The equations governing this minimum resonance energy (see, for example, Equation 12 from Omura and Zhao (2013)) allow for arbitrarily low resonance energies for waves with frequencies close to the local ion gyrofrequencies (e.g., Figure 2 from Omura and Zhao (2013)) or for waves occurring in particularly dense plasma regions, such as just inside the plasmapause. In addition, recent theoretical results have introduced further mechanisms to lower the minimum resonance energy (e.g., Denton et al., 2019; Zhang et al., 2019).

The experimental evidence for a 1-2 MeV limit is not conclusive either. Since the very early days of EMIC research, there have been hints, if not necessarily direct evidence, to suggest that EMIC waves are capable of interacting with electrons with sub-MeV energies. Both Troitskaya (1961) and Heacock (1967) noted that IPDP (intervals of pulsations diminishing in period) waves, a subset of EMIC waves, coincided with sharp increases in cosmic noise absorption (CNA) signatures in ground-based riometers, most likely indicative of sub-MeV electron precipitation. Gendrin et al. (1967) noted that these IPDP waves also tended to coincide with sudden drops in trapped energetic (100s of keV) electron flux, based on observations from the Electron 1 and Transit 5E-1 satellites. At the time, these signatures were not attributed to wave-driven electron precipitation, and these observations were apparently not followed up on in any great detail.

In the past few decades, a number of experimental observations supporting the idea of sub-MeV electron precipitation have emerged. While some of these results are from indirect measurements such as balloon-based x-rays (e.g. Blum et al., 2015; Millan et al., 2007; Woodger et al., 2015, 2018), many of these include direct measurements of precipitating electron flux from satellites such as the Polar-Orbiting Operational Environmental Satellite (POES) constellation (e.g. M. A. Clilverd et al., 2015; Rodger et al., 2015; Hendry et al., 2017, 2019), and the Firebird-II cubesat satellites (Capannolo et al., 2019, 2021). One of the most important of these results was the broad survey of POES precipitation bursts by Hendry et al. (2017), which showed that not only was sub-MeV precipitation by EMIC waves possible, but it was the dominant form of EMIC-EP seen in the POES dataset. This result seems to be in direct contradiction to the aforementioned statistical and trapped flux studies suggesting purely relativistic scattering, however as noted above this is a result supported by multiple independent studies using different instruments.

A solution to this apparent contradiction was posited by Hendry et al. (2021), who showed that it was possible for both EMIC-induced sub-MeV electron precipitation and an experimentally determined multi-MeV "limit" to co-exist. By combining electron energy spectra derived from observed POES precipitation fluxes with a trapped flux model, Hendry et al. argued that strong sub-MeV EEP could occur whilst barely affecting the sub-MeV trapped flux populations, whereas the > 1 MeV EEP component of the spectra could still generate significant relativistic and ultra-relativistic flux dropouts. However, no experimental results were provided to support this suggestion in that study.

In this study we analyse GPS satellite dosimeter measurements of trapped electron fluxes in order to look for evidence of sub-MeV EMIC driven dropouts in trapped electron flux. We combined the dosimeter measurements with an extensive database of EMIC wave occurrence, and undertake a superposed epoch analysis to identify dropout levels over a range of electron energies. In the next section, we will briefly outline the instrumentation used in this study. This is followed in Section 3 by a more in-depth discussion of the apparent contradiction between the theoretical limits of EMIC-electron interactions and experimental EEP observations. In Section 4, we carry out a broad statistical investigation of GPS trapped flux measurements to determine if there is any evidence of an electron flux dropout at sub-MeV energies. Finally, we discuss these results in Section 5.

2 Instrumentation

The main instrument used in this study is the Combined X-ray Dosimeter (CXD) instrument carried by most of the satellites in the Global Positioning System (GPS) constellation. As of writing, there are CXD data publicly available for 21 of the GPS satellites from 2001/02/18 to 2019/01/05 – in total there are 64,370 instrument days worth of data (roughly 176 years). Although in theory these instruments can sample with a variable sample-rate, in practise this is set to 240 s. The CXD instrument measures electrons across 11 energy channels from roughly 120 keV to >6 MeV. These counts are background corrected and fluxes are estimated using a forward modelling procedure and have been cross-calibrated against Van Allen Probes measurements (Morley et al., 2016). The public data product (S. Morley et al., 2017) provides differential omnidirectional flux values at 15 energies from 120 keV up to 10 MeV, which we use in this study. For more information, including fit quality checks, see Smirnov et al. (2020) and references therein.

2.1 Constructing an EMIC event database

To construct an EMIC event database, we use data from the POES constellation, specifically the Medium Energy Proton and Electron Detector (MEPED) suite of particle detectors. The MEPED instrument, its flaws, and its usefulness in detecting EMIC-EP, has been discussed extensively in the literature (Evans & Greer, 2000; Rodger et al., 2010; Yando et al., 2011; Carson et al., 2013; Peck et al., 2015; Sandanger et al., 2015; Ødegaard et al., 2016; Hendry et al., 2017, 2021).

A list of EMIC-EP events, used to compare the GPS trapped flux data, was generated with the EMIC REP detection algorithm derived by Carson et al. (2013). The algorithm and the resulting database of events it creates have been discussed thoroughly in the literature, including demonstrating the link between these REP events and EMIC wave activity (Hendry et al., 2016), investigating the energy range of the events (Hendry et al., 2017), and investigating the potential impact of these events on the radiation belts and upper atmosphere (Hendry et al., 2021).

In each of the above papers, the database of EMIC events included data up until the end of 2015. Here, we have rerun the Carson et al. (2013) algorithm to include POES MEPED data up until the end of 2019, which includes data from the final satellite in the current POES era, METOP-C (also called METOP-03). The inclusion of these data extends the REP event database to 5096 events, compared to the 3777 events studied by the aforementioned papers. Some of these events fall outside the current publicly available GPS CXD dataset, leaving 4687 events (i.e., $\sim$92% of the original set). It is also worth noting that since the decommissioning of the NOAA-16 and NOAA-17 satellites in 2014 and 2013 respectively, two "blind-spots" have opened up in the MLT coverage of the POES satellites at magnetic noon (12-15 MLT, all L-shells) and magnetic midnight (00–03 MLT, $L < 5$, within which very few measurements are made. This should not affect our results due to the availability of many years of data prior to the loss of these satellites.

3 The EMIC contradiction: efficiency vs. impact

Perhaps one of the biggest reasons for the apparent energy-limit contradiction between the theory and observations of EMIC-EP is the intent behind the investigations producing these results. When considering this precipitation from a theoretical point of view, typically we are interested in the *efficiency* of the process, as opposed to the total scattered electron population; the same is also true of investigations into trapped flux changes. If a wave is capable of scattering only (say) 0.1% of electrons at low energies, but can scatter close to 100% of electrons at high energies, then from a theoretical perspective we are likely to be primarily interested in the efficient high energy process, rather than the inefficient low energy process. Similarly, an efficient process is much more likely to present a visible change in trapped flux than an inefficient process, particularly for case studies.

In comparison, if we are interested in the *impact* of EMIC-EP on atmospheric chemistry, then the question of efficiency becomes somewhat secondary to the total magnitude of electrons precipitated. Typically the population of low energy trapped electrons is several orders-of-magnitude larger than the high energy population. Even if a wave can only scatter (say) 0.1% of electrons at low energies compared to 100% at high energies, if the population of low energy electrons is several orders-of-magnitude larger than the high energy population then the low energy electrons may be just as important, if not more important, than the high energy electrons from an atmospheric perspective. Thus, in terms of the impact of these events it may be that the efficiency of the processes involved is less important than the size of the reservoir of trapped electrons at various energies.

Recognising this distinction between the efficiency of the EMIC-electron scattering process and the impact of the resulting precipitation gives us a surprisingly simple solution to our contradiction. The answer comes from the possibility of a small amount of inefficient scattering below the minimum resonance energy generating a significant level of sub-MeV EEP while only causing small changes to the trapped flux. Given the limited nature of current measures of trapped flux, this inefficient loss may be missed in single-event case studies such as those carried out by Usanova et al. (2014) and Shprits et al. (2016). In theory, however, it should be visible if we consider trapped flux changes from a broader, more statistical perspective.

4 GPS Observed Dropouts

If our suggestion of inefficient scattering by EMIC waves below the minimum resonance energy is correct, then with the right data analysis we should be able to observe changes in trapped electron flux at sub-MeV energies, while also confirming relativistic changes. On a case by case basis, the 4-minute resolution of the CXD data can make it difficult to distinguish finer details of the trapped flux, and in theory the higher time resolution of the Van Allen Probe or Arase satellite trapped flux measurements would offer far greater time resolution. However, by their very nature the GPS satellites are *global*, and thus offer very good coverage in MLT; for our purposes this improved coverage is more important than fine time-resolution.

To get an idea of the "typical" response of the trapped flux levels in the radiation belts to an EMIC wave event, we consider our events from a statistical perspective, using superposed epoch analysis (SEA) to extract the underlying behaviour from the data. This approach is widely used and well-documented within the space physics literature (e.g., S. K. Morley et al., 2010; Rodger et al., 2019).

The most important feature of SEA is a well defined epoch. With a poorly defined epoch, the data may become "smeared out", and the result will not represent as accurately the actual underlying trends in the data. We use the timing of the REP triggers from the Carson et al. (2013) algorithm as our epoch definition. We suspect that our epoch definition is not perfect for this task, in the sense that it does not necessarily represent the true onset of the wave events. If, however, the impact of EMIC-driven scattering on the radiation belts is longer-lived than the uncertainty in the REP trigger timing in the database, we assume it will not affect the overall picture we get from the SEA.

For calculating the SEA, we bin the GPS data according to time, L-shell, and MLT. We use 15 min bins, which gives us a good number of events per bin, without limiting the resolution of the statistical analysis. We investigate the data from 10 days prior to the event to 15 days after the event; this provides an indication of the state of the radiation belts before the event (i.e., a "non-disturbed" level of flux), and lets us determine the recovery period of the belts following these events.

We examine four MLT sectors: dawn (00-06 MLT), morning (06-12 MLT), afternoon (12-18 MLT), and dusk (18-24 MLT). For high energy electrons with short orbital drift-periods, we do not expect to see timing offsets in the dropouts across different MLT sectors — in other words, we do not expect to be able to see the dropouts "drift" in MLT (cf. the drift of substorm-related dropouts seen by Rodger et al. (2019)). The combination of the uncertainty of the event onset time with regards to the epoch time and the rapid drift rate of the higher energy electrons means that, at least in theory, there should be little difference between the MLT sectors.

To investigate L-shell characteristics of the dropout events we use L^* as opposed to McIlwain's L, calculated using the Tsyganenko and Sitnov (2005) (TS05) magnetic field model. Due to the large amounts of data that must be processed to produce L^* for the entire GPS dataset, we used the LANLstar neural network method for estimating L^* instead of a full drift-shell calculation (Yu et al., 2012), calculated using SpacePy (Morley et al., 2011; Morley et al., 2019). With regards to binning L^*, we are limited somewhat by the L-shells sampled by the GPS satellite. Due to the orbits of the satellites, our observations are restricted to $L^* > 4$. At higher L^* values fluxes are typically small, and the number of observations are fewer. To ensure that our statistics are valid and meaningful, we restrict ourselves to GPS observations in the range $4 \leq L^* \leq 5$, also excluding events that occur outside this range — this leaves us with 875 events ($\sim 20\%$ of the database) to investigate. Over this L-shell range, the GPS satellites are constrained to magnetic latitude close to the magnetic equator, and thus the fluxes measured are a fair representation of the total flux present in the belts at these L-shells (c.f., Figure 3 of Morley et al. (2016)). These events are most common around 18-22 MLT, similar to the full database, although due to the L-shell filtering we see a reduction in pre-midnight events, which tend towards higher L-shells.

For our primary statistic, we use a median to estimate the central trend of the trapped flux data; the upper- and lower-quartiles of the data are also calculated. Finally, we also calculate the 95% confidence interval of the median and quartile timeseries, to determine if any effects we see are statistically meaningful. Due to the nature of the flux data we cannot assume normality, and thus a typical t-statistic confidence interval would be misleading. Instead, we calculate the 95% *bootstrap* confidence intervals of the median and quartiles. We calculate these using the MATLAB `bootci` function, with 1000 bootstrap samples per statistic and using the bias-corrected and accelerated bootstrap method Efron (1987).

To determine the change from our events compared to non-disturbed conditions, we estimate the non-disturbed flux by repeating the above analysis using a set of "random" epochs. We generate these by adding a random offset uniformly distributed in the range (-30,30) days to each event epoch — this ensures that the temporal distribution of the random epochs matches that of the true epochs.

Finally, we investigate the geomagnetic conditions at the time of these epochs by calculating the SEA of the SYM-H and *SME* (SuperMAG Auroral Electrojet, Gjerloev (2012)) indices — we use SYM-H instead of *Dst* for the increased time resolution (1 min vs 1 hr) and use *SME* instead of *AE* due to (at the time of writing) the lack of provisional AE data for most of 2018.

4.1 SEA Results

A selection of the results from our analysis are shown in Figure 1. Figures 1(a) and (b) show the variation of the SME and SYM-H indices around the event time, with the median shown in black, the interquartile ranges in light-red, and the 95% confidence intervals of these in blue and red respectively. An estimated non-disturbed flux, calculated using the random epochs, is shown in yellow. Although there is a clear variation in SYM-H at the event time (left panel), the median value does not drop below -15 nT, suggesting a lack of significant geomagnetic storm activity. By contrast, the SME index (left panel) shows a sharp spike at the zero-epoch, indicating that our events are strongly associated with substorm activity — this is to be expected, with evidence suggesting that substorm-driven ion injections are important drivers of EMIC wave activity (Remya et al., 2018; H. Chen et al., 2020).

Figures 1(c-h) shows the SEA of the GPS electron flux for $4 < L^* < 5$, following the same color format as Figure 1(a-b). As expected, we found very little difference between the MLT sectors, and here we show only the 18–24 MLT sector.

At the lowest energies (120 keV, Figure 1(a)), we see a roughly 50% drop in the trapped electron fluxes starting on the zero-epoch day, lasting less than a day, and followed by a rapid growth in the trapped fluxes to above pre-event levels. The enhancement of flux above the non-disturbed levels lasts for approximately 5 days. At 600 keV (Figure 1(b)), we see a similar drop in the trapped flux of $\sim 60\%$, but this time followed by a slower recovery to pre-event flux levels over the course of 5-10 days. At 1 MeV (Figure 1(c)), we see a similar sharp drop in the trapped flux ($\sim 60\%$), followed by a recovery over the course of several days. At ultra-relativistic energies (Figure 1(d-f)) we see much stronger flux decreases — peaking at 95% loss for 4 MeV fluxes — following the same drop-recovery process. At these highest energies the decrease in flux lasts for ~ 2 days.

We suggest the following chain of events is taking place for our epochs:

1. In the lead up to the zero-epoch, we observe a "calm before the storm" type effect (M. Clilverd et al., 1993; Borovsky & Denton, 2009), as seen by the quietening of the indices in Figures 1(a) and (b) before the zero-epoch.
2. An EMIC event is triggered, leading to rapid scattering loss of relativistic and sub-relativistic electrons. In the case of ultra-relativistic electrons, this leads to a significant, order of magnitude drop in trapped fluxes, while at lower, sub-relativistic electrons the decrease in trapped fluxes is much smaller.
3. Following the EMIC event, substorm-related acceleration processes (e.g., Meredith et al., 2002) refill the belts over the course of several days, with the rate of replenishment being strongly energy dependent — sub-relativistic electrons are rapidly accelerated well above pre-storm levels, while ultra-relativistic electrons are only slowly replenished.
4. As the disturbed period abates, the enhanced fluxes slowly return to non-disturbed levels 5-10 days after the EMIC event (e.g., Rodger et al., 2016).

To ensure that the flux variations seen in our analysis were not simply due to substorm activity, we repeated the analysis above using the onset of a substorm as the defining epoch, using the SuperMAG substorm database to generate a list of substorms from 1998–2019. To reduce overlap between events, we filtered this list down to a list of 6276 "clustered" (or "recurrent") substorms (cf. Cresswell-Moorcock et al. (2013) and Rodger et al. (2019)). The results of this analysis are plotted in Figure S1 in the Supplementary Material. The variation of the geomagnetic indices is very similar between the two event types, with the substorm epochs showing slightly more active geomagnetic conditions. We also see very similar flux increases for times after the zero epoch, supporting our theory that the flux recovery seen in Figures 1(c-h) is driven by substorm-related processes. However, at the zero epoch there are significant differences in the response of the trapped flux for each event type — whereas the EMIC epochs show a very strong, sudden dropout around the zero-epoch, the substorms show only a very small change in

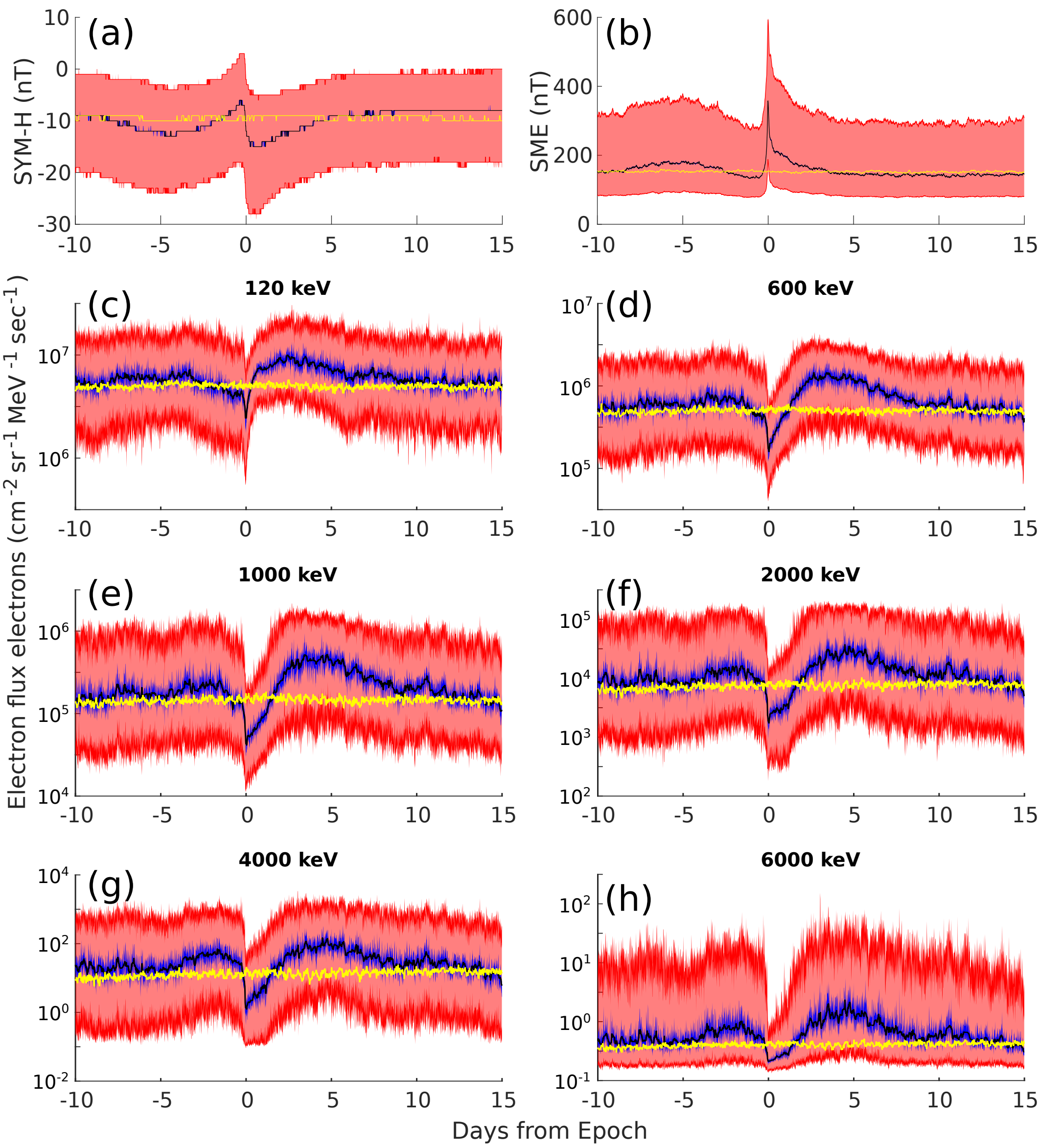

Figure 1. Response of the (a) SYM-H index, (b) SME index, and (c-h) GPS CXD-measured trapped electron flux to EMIC wave activity. GPS CXD fluxes are shown for energies from 120–6000 keV for $4 < L^* < 5$ and 18–24 MLT. In each plot the black line indicates the median flux for the combined event list, with the blue region indicting the 95% bootstrapped confidence interval. The light red region indicates the interquartile range of the flux, with dark red indicating the 95% confidence interval of this statistic. The yellow line indicates the estimated non-disturbed flux levels. Due to the large number of events involved, the confidence intervals are almost indistinguishable from the ranges themselves.

flux. This suggests that the flux change we are seeing is not purely due to substorm-related changes in the radiation belts.

4.1.1 Event MLT examination

There was little variation in the characteristics of the events in the above analysis when observed by the satellites in different MLT sectors. This is not altogether surprising, given the rapid drift periods of the electrons in question combined with the long accumulation period of the GPS CXD instruments. If, however, we investigate the events and the trapped flux based on the MLT sector of the *events*, we see rather stark changes, suggesting that different scattering conditions could occur when the EMIC events are triggered at different MLT.

In the following analysis, we repeated the above procedure, grouping the data based on the MLT of the events, rather than the MLT of the GPS satellites. We consider 8 MLT sectors, each 3 hr wide. For each sector, we select all events in the database that occur in that sector, and consider the average trapped flux from all of the GPS satellites at that time. In other words, we do not bin the GPS data according to satellite MLT but rather consider the radiation belts as a whole. This decision was primarily to ensure that we had enough data points to extract meaningful statistics. The results are shown in Figure 2.

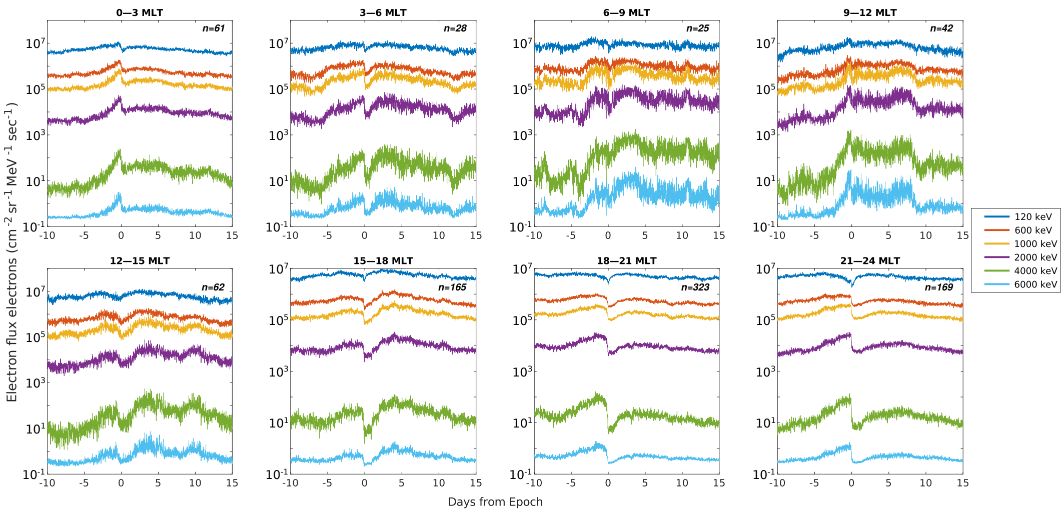

Figure 2. Median GPS CXD measured response of trapped electrons to EMIC wave activity, at energies from 120–6000 keV, binned based on the MLT of the POES precipitation events in 3 hr MLT bins.

For events occurring the morning-to-noon sectors (6–12 MLT, Figures 2(c–e)), we see an increase in trapped electron flux starting roughly 5 days before the zero-epoch, but see relatively little change in trapped flux at the event time. This may be in part due to the small number of events in this region (roughly 11% of the total database), however it may also be indicative of a reduction in the scattering efficiency due to an MLT dependence of local plasma conditions during the EMIC events (e.g., Summers & Thorne, 2003; Meredith et al., 2003).

For events in the dawn and afternoon-to-evening sectors (03–06 MLT, 12–18, Figures 2(b, f-g)) we see an initial increase in trapped flux, then a strong decrease in the trapped flux across all energies, followed by a replenishment/acceleration taking place over the course of several days.

For events in the dusk-midnight sector (18–03 MLT, Figures 2(h,a)), we again see a build-up of flux before the zero-epoch, followed by a strong, rapid decrease in the trapped flux. Unlike events in the other sectors, there is much slower replenishment following the zero-epoch, suggesting that fluxes may stay suppressed for long periods after their loss.

5 Discussion

From our results, it is clear that significant trapped electron flux dropouts are occurring across a broad range of energies concurrently with our EMIC trigger events, including sub-MeV energies as low as 120 keV. Although this is much lower than is considered possible through traditional resonant scattering, it agrees with previously published results from the Van Allen Probes by Rodger et al. (2015) and Hendry et al. (2019), both of whom observed EMIC-related trapped flux dropouts down to energies around 100–200 keV. Importantly, however, the recovery from these low energy dropouts in the GPS data is very rapid, returning to pre-storm levels less than a day after the zero-epoch. This potentially explains why these dropouts were not seen in previously published case-studies, due to the longer timescales used in such works. In contrast, ultra-relativistic decreases due to EMIC waves are observed to last from days to weeks, and exhibit substantially larger flux loss — this makes them easier to detect than sub-MeV events. We note that the ultra-relativistic flux recovery timescales seen in Figure 1 are strikingly similar to those shown in Figures 3(d-f) of Usanova et al. (2014).

Although previous work has strongly linked the POES precipitation events used in this study with EMIC activity (Hendry et al., 2016), as this analysis has no direct wave measurements, we cannot guarantee that the observed electron dropouts are driven solely by EMIC-wave activity. However, previous studies have shown that EMIC waves are capable of driving EEP at such low energies (e.g., Hendry et al., 2019). Furthermore, in several cases where in-situ wave observations of these events was possible, no alternative explanation in terms of our wave sources was found (e.g., Rodger et al., 2015; Hendry et al., 2017). Thus is seems likely that EMIC waves are at the very least a major driver of the flux dropouts we have seen here.

One of the limitations of our study, or indeed any statistical investigation of EMIC waves, is that we cannot be sure of the onset time of the individual EMIC wave events. As we have based our zero-epoch on the timing of the precipitation triggers seen by POES, our epochs are based on when the POES satellites happen to fly through the event region. As has been observed in previous studies , EMIC events may last for many hours(e.g., Engebretson et al., 2015; Blum et al., 2020), and our POES triggers may occur anywhere within these events (e.g., Hendry et al., 2016). This likely explains why we typically see the flux levels drop just before the zero-epoch.

Due to orbits of the GPS satellites, in this study we limited our investigations to $4 \leq L^* \leq 5$. Although GPS observations exist at higher L-shells, within these regions the magnetic latitude of the satellites tends away from the equator, limiting our ability to study the entire trapped flux population of the radiation belts.

Our results provide experimental evidence to explain the contradicting results surrounding EMIC REP energies found in the literature. When viewed from the perspective of trapped fluxes, the primary long-term losses related to EMIC wave activity are relativistic and ultra-relativistic. This is in part due to the efficient resonant scattering that occurs at these energies, but also due to the slow replenishment of these electrons. In contrast, the relatively inefficient scattering of sub-MeV electrons combined with the rapid replenishment of any losses means that, from a radiation belt dynamics point of view, these losses are relatively unimportant. However, when viewed from an atmospheric perspective, the inefficient but quantitatively large precipitation of sub-MeV electrons by EMIC waves is potentially very important and should not be ignored.

One of the core assumptions of our overall result is the existence of a process by which EMIC waves are able to drive inefficient electron scattering at energies below the minimum resonance energy. One such possibility is that we are seeing evidence of non-resonant scattering, previously described by L. Chen et al. (2016), in which strong EMIC waves with sharp wave-fronts are able cause the scattering loss of electrons at energies below the minimum resonance energy. To the authors' knowledge, there has not been any in-depth investigation of this mechanism beyond the original paper, although non-resonant scattering was cited by Hendry et al. (2019) as a possible explanation for weak sub-resonant electron loss present in their test-particle simulation. Another possibility is scattering due to a combination of hydrogen and helium band EMIC waves, as suggested by Denton et al. (2019). Clearly further research is needed to determine if non-resonant scattering can explain the observed sub-resonant losses, or if some other mechanism is required.

6 Conclusions

In this study, we examined the impact of EMIC waves on trapped electron populations across a broad range of energies using the GPS CXD instruments. As well as providing strong statistical support for EMIC-driven depletion of trapped ultra-relativistic electrons, we have also shown that this loss extends down to sub-MeV energies. This is a much lower energy for trapped changes than previously observed in the literature, but is consistent with the growing body of studies showing sub-MeV EMIC-driven EEP.

Acknowledgments
The authors would like to thank the CXD team at Los Alamos National Laboratory who develop, maintain, operate, and process the GPS CXD data used in this study. The GPS CXD data and documentation used in this study can be found at https://www.ngdc.noaa.gov/stp/space-weather/satellite-data/satellite-systems/gps/. The authors wish to thank the personnel who developed, maintain, and operate the NOAA/POES spacecraft; the POES MEPED data can be found at https://satdat.ngdc.noaa.gov/sem/poes/. The authors acknowledge the SuperMAG collaborators (http://supermag.jhuapl.edu/info/?page=acknowledgement). MAC would like to acknowledge support for this work from the Natural Environment Research Council, NERC Highlight Topic Grant #NE/P01738X/1 (Rad-Sat). Contributions by SKM were performed under the auspices of the U.S. Department of Energy, with partial support from the Laboratory Directed Research and Development (LDRD) program, awards 20150127ER and 20190262ER.

References

Blum, L. W., Halford, A., Millan, R., Bonnell, J. W., Goldstein, J., Usanova, M., ... Li, X. (2015). Observations of coincident emic wave activity and duskside energetic electron precipitation on 18–19 january 2013. *Geophysical Research Letters*, *42*(14), 5727-5735. Retrieved from `https://agupubs.onlinelibrary.wiley.com/doi/abs/10.1002/2015GL065245` doi: https://doi.org/10.1002/2015GL065245

Blum, L. W., Remya, B., Denton, M. H., & Schiller, Q. (2020). Persistent emic wave activity across the nightside inner magnetosphere. *Geophysical Research Letters*, *47*(6), e2020GL087009. Retrieved from `https://agupubs.onlinelibrary.wiley.com/doi/abs/10.1029/2020GL087009` (e2020GL087009 2020GL087009) doi: https://doi.org/10.1029/2020GL087009

Borovsky, J. E., & Denton, M. H. (2009). Electron loss rates from the outer radiation belt caused by the filling of the outer plasmasphere: The calm before the storm. *Journal of Geophysical Research: Space Physics*, *114*(A11). Retrieved from http://dx.doi.org/10.1029/2009JA014063 doi: 10.1029/2009JA014063

Capannolo, L., Li, W., Ma, Q., Chen, L., Shen, X.-C., Spence, H., ... others (2019). Direct observation of subrelativistic electron precipitation potentially driven by emic waves. *Geophysical Research Letters*, *46*(22), 12711–12721.

Capannolo, L., Li, W., Spence, H., Johnson, A. T., Shumko, M., Sample, J., & Klumpar, D. (2021). Energetic electron precipitation observed by firebird-ii potentially driven by emic waves: Location, extent, and energy range from a multievent analysis. *Geophysical Research Letters*, *48*(5), e2020GL091564. Retrieved from https://agupubs.onlinelibrary.wiley.com/doi/abs/10.1029/2020GL091564 (e2020GL091564 2020GL091564) doi: https://doi.org/10.1029/2020GL091564

Carson, B. R., Rodger, C. J., & Clilverd, M. A. (2013). POES satellite observations of EMIC-wave driven relativistic electron precipitation during 1998-2010. *Journal of Geophysical Research: Space Physics*, *118*(1), 232–243. Retrieved from http://dx.doi.org/10.1029/2012JA017998 doi: 10.1029/2012JA017998

Chen, H., Gao, X., Lu, Q., Tsurutani, B. T., & Wang, S. (2020). Statistical evidence for emic wave excitation driven by substorm injection and enhanced solar wind pressure in the earth's magnetosphere: Two different emic wave sources. *Geophysical Research Letters*, *47*(21), e2020GL090275. Retrieved from https://agupubs.onlinelibrary.wiley.com/doi/abs/10.1029/2020GL090275 (e2020GL090275 2020GL090275) doi: https://doi.org/10.1029/2020GL090275

Chen, L., Thorne, R. M., & Bortnik, J. (2011). The controlling effect of ion temperature on EMIC wave excitation and scattering. *Geophysical Research Letters*, *38*(16). Retrieved from http://dx.doi.org/10.1029/2011GL048653 doi: 10.1029/2011GL048653

Chen, L., Thorne, R. M., Bortnik, J., & Zhang, X.-J. (2016). Nonresonant interactions of electromagnetic ion cyclotron waves with relativistic electrons. *Journal of Geophysical Research: Space Physics*, *121*(10), 9913–9925. Retrieved from http://dx.doi.org/10.1002/2016JA022813 doi: 10.1002/2016JA022813

Clilverd, M., Clark, T., Smith, A., & Thomson, N. (1993). Observation of a decrease in mid-latitude whistler mode signal occurrence prior to geomagnetic storms. *Journal of Atmospheric and Terrestrial Physics*, *55*(10), 1479 - 1485. Retrieved from http://www.sciencedirect.com/science/article/pii/002191699390113D doi: http://dx.doi.org/10.1016/0021-9169(93)90113-D

Clilverd, M. A., Duthie, R., Hardman, R., Hendry, A. T., Rodger, C. J., Raita, T., ... Milling, D. K. (2015). Electron precipitation from EMIC waves: A case study from 31 May 2013. *Journal of Geophysical Research: Space Physics*, *120*(5), 3618–3631. Retrieved from http://dx.doi.org/10.1002/2015JA021090 doi: 10.1002/2015JA021090

Cresswell-Moorcock, K., Rodger, C. J., Kero, A., Collier, A. B., Clilverd, M. A., Häggström, I., & Pitkänen, T. (2013). A reexamination of latitudinal limits of substorm-produced energetic electron precipitation. *Journal of Geophysical Research: Space Physics*, *118*(10), 6694–6705. Retrieved from http://dx.doi.org/10.1002/jgra.50598 doi: 10.1002/jgra.50598

Denton, R., Ofman, L., Shprits, Y., Bortnik, J., Millan, R., Rodger, C., ... Komar, C. (2019). Pitch angle scattering of sub-MeV relativistic electrons by electromagnetic ion cyclotron waves. *Journal of Geophysical Research: Space Physics*, *0*(ja). Retrieved from https://agupubs.onlinelibrary.wiley.com/doi/abs/10.1029/2018JA026384 doi: 10.1029/2018JA026384

Efron, B. (1987). Better bootstrap confidence intervals. *Journal of the American sta-*

tistical Association, *82*(397), 171–185.

Engebretson, M. J., Posch, J. L., Wygant, J. R., Kletzing, C. A., Lessard, M. R., Huang, C.-L., ... Shiokawa, K. (2015). Van Allen probes, NOAA, GOES, and ground observations of an intense EMIC wave event extending over 12 h in magnetic local time. *Journal of Geophysical Research: Space Physics*. Retrieved from `http://dx.doi.org/10.1002/2015JA021227` doi: 10.1002/2015JA021227

Evans, D. S., & Greer, M. S. (2000). *Polar Orbiting Environmental Satellite Space Environment Monitor-2: Instrument Description and Archive Data Documentation.* US Department of Commerce, National Oceanic and Atmospheric Administration, Oceanic and Atmospheric Research Laboratories, Space Environment Center.

Gendrin, R., Lacourly, S., Troitskaya, V., Gokhberg, M., & Shepetnov, R. (1967). Caracteristiques des pulsations irregulieres de periode decroissante (ipdp) et leurs relations avec les variations du flux des particules piegees dans la magnetosphere. *Planetary and Space Science*, *15*(8), 1239–1240.

Gjerloev, J. W. (2012). The SuperMAG data processing technique. *Journal of Geophysical Research: Space Physics*, *117*(A9). Retrieved from `https://agupubs.onlinelibrary.wiley.com/doi/abs/10.1029/2012JA017683` doi: https://doi.org/10.1029/2012JA017683

Heacock, R. (1967). Two subtypes of type Pi micropulsations. *Journal of Geophysical Research*, *72*(15), 3905–3917.

Hendry, A. T., Rodger, C. J., & Clilverd, M. A. (2017). Evidence of sub-MeV EMIC-driven electron precipitation. *Geophysical Research Letters*, *44*(3), 1210–1218. Retrieved from `http://dx.doi.org/10.1002/2016GL071807` doi: 10.1002/2016GL071807

Hendry, A. T., Rodger, C. J., Clilverd, M. A., Engebretson, M. J., Mann, I. R., Lessard, M. R., ... Milling, D. K. (2016). Confirmation of EMIC wave driven relativistic electron precipitation. *Journal of Geophysical Research: Space Physics*. Retrieved from `http://dx.doi.org/10.1002/2015JA022224` doi: 10.1002/2015JA022224

Hendry, A. T., Santolik, O., Kletzing, C. A., Rodger, C. J., Shiokawa, K., & Baishev, D. (2019). Multi-instrument Observation of Nonlinear EMIC-Driven Electron Precipitation at sub–MeV Energies. *Geophysical Research Letters*, *46*(13), 7248-7257. Retrieved from `https://agupubs.onlinelibrary.wiley.com/doi/abs/10.1029/2019GL082401` doi: 10.1029/2019GL082401

Hendry, A. T., Seppälä, A., Rodger, C. J., & Clilverd, M. A. (2021). Impact of emic-wave driven electron precipitation on the radiation belts and the atmosphere. *Journal of Geophysical Research: Space Physics*, *126*(3), e2020JA028671. Retrieved from `https://agupubs.onlinelibrary.wiley.com/doi/abs/10.1029/2020JA028671` (e2020JA028671 2020JA028671) doi: https://doi.org/10.1029/2020JA028671

Loto'aniu, T. M., Thorne, R. M., Fraser, B. J., & Summers, D. (2006). Estimating relativistic electron pitch angle scattering rates using properties of the electromagnetic ion cyclotron wave spectrum. *Journal of Geophysical Research: Space Physics*, *111*(A4). Retrieved from `http://dx.doi.org/10.1029/2005JA011452` doi: 10.1029/2005JA011452

Matthes, K., Funke, B., Andersson, M. E., Barnard, L., Beer, J., Charbonneau, P., ... others (2017). Solar forcing for CMIP6 (v3. 2). *Geoscientific Model Development*, *10*(6), 2247.

Meredith, N. P., Horne, R. B., Iles, R. H. A., Thorne, R. M., Heynderickx, D., & Anderson, R. R. (2002). Outer zone relativistic electron acceleration associated with substorm-enhanced whistler mode chorus. *Journal of Geophysical Research: Space Physics*, *107*(A7), SMP 29-1-SMP 29-14. Retrieved from `https://agupubs.onlinelibrary.wiley.com/doi/abs/10.1029/`

2001JA900146 doi: https://doi.org/10.1029/2001JA900146
Meredith, N. P., Thorne, R. M., Horne, R. B., Summers, D., Fraser, B. J., & Anderson, R. R. (2003). Statistical analysis of relativistic electron energies for cyclotron resonance with EMIC waves observed on CRRES. *Journal of Geophysical Research: Space Physics*, *108*(A6). Retrieved from http://dx.doi.org/10.1029/2002JA009700 doi: 10.1029/2002JA009700
Millan, R. M., Lin, R. P., Smith, D. M., & McCarthy, M. P. (2007). Observation of relativistic electron precipitation during a rapid decrease of trapped relativistic electron flux. *Geophysical research letters*, *34*(10).
Morley, S., Sullivan, J., Carver, M., Kippen, R., Friedel, R., Reeves, G., & Henderson, M. (2017). Energetic particle data from the global positioning system constellation. *Space Weather*, *15*(2), 283–289.
Morley, S. K., Friedel, R. H. W., Spanswick, E. L., Reeves, G. D., Steinberg, J. T., Koller, J., ... Noveroske, E. (2010). Dropouts of the outer electron radiation belt in response to solar wind stream interfaces: global positioning system observations. *Proceedings of the Royal Society of London A: Mathematical, Physical and Engineering Sciences*, *466*(2123), 3329–3350. Retrieved from http://rspa.royalsocietypublishing.org/content/466/2123/3329 doi: 10.1098/rspa.2010.0078
Morley, S. K., Koller, J., Welling, D. T., Larsen, B. A., Henderson, M. G., & Niehof, J. T. (2011). Spacepy - A Python-based library of tools for the space sciences. In *Proceedings of the 9th Python in science conference (SciPy 2010).* Austin, TX.
Morley, S. K., Niehof, J. T., Welling, D. T., Larsen, B. A., Haiducek, J., Killick, P., ... Henderson, M. G. (2019, October). *spacepy/spacepy: 0.2.1.* Zenodo. Retrieved from https://doi.org/10.5281/zenodo.3252523 doi: 10.5281/zenodo.3252523
Morley, S. K., Sullivan, J. P., Henderson, M. G., Blake, J. B., & Baker, D. N. (2016). The global positioning system constellation as a space weather monitor: Comparison of electron measurements with van allen probes data. *Space Weather*, *14*(2), 76–92.
Omura, Y., & Zhao, Q. (2013). Relativistic electron microbursts due to nonlinear pitch angle scattering by EMIC triggered emissions. *Journal of Geophysical Research: Space Physics*, *118*(8), 5008–5020.
Peck, E. D., Randall, C. E., Green, J. C., Rodriguez, J. V., & Rodger, C. J. (2015). POES MEPED differential flux retrievals and electron channel contamination correction. *Journal of Geophysical Research: Space Physics*, *120*(6), 4596–4612. Retrieved from http://dx.doi.org/10.1002/2014JA020817 doi: 10.1002/2014JA020817
Remya, B., Sibeck, D. G., Halford, A. J., Murphy, K. R., Reeves, G. D., Singer, H. J., ... Thaller, S. A. (2018). Ion injection triggered EMIC waves in the earth's magnetosphere. *Journal of Geophysical Research: Space Physics*, *123*(6), 4921-4938. Retrieved from https://agupubs.onlinelibrary.wiley.com/doi/abs/10.1029/2018JA025354 doi: 10.1029/2018JA025354
Rodger, C. J., Carson, B. R., Cummer, S. A., Gamble, R. J., Clilverd, M. A., Green, J. C., ... Berthelier, J.-J. (2010). Contrasting the efficiency of radiation belt losses caused by ducted and nonducted whistler-mode waves from ground-based transmitters. *Journal of Geophysical Research: Space Physics (1978–2012)*, *115*(A12).
Rodger, C. J., Cresswell-Moorcock, K., & Clilverd, M. A. (2016). Nature's grand experiment: Linkage between magnetospheric convection and the radiation belts. *Journal of Geophysical Research: Space Physics*, *121*(1), 171-189. Retrieved from https://agupubs.onlinelibrary.wiley.com/doi/abs/10.1002/2015JA021537 doi: https://doi.org/10.1002/2015JA021537
Rodger, C. J., Hendry, A. T., Clilverd, M. A., Kletzing, C. A., Brundell, J. B.,

& Reeves, G. D. (2015). High-resolution In-situ Observations of Electron Precipitation-Causing EMIC Waves. *Geophysical Research Letters*. Retrieved from http://dx.doi.org/10.1002/2015GL066581 doi: 10.1002/2015GL066581

Rodger, C. J., Turner, D. L., Clilverd, M. A., & Hendry, A. T. (2019). Magnetic local time-resolved examination of radiation belt dynamics during high-speed solar wind speed-triggered substorm clusters. *Geophysical Research Letters*, *46*(17-18), 10219-10229. Retrieved from https://agupubs.onlinelibrary.wiley.com/doi/abs/10.1029/2019GL083712 doi: https://doi.org/10.1029/2019GL083712

Sandanger, M. I., Ødegaard, L.-K. G., Nesse Tyssøy, H., Stadsnes, J., Søraas, F., Oksavik, K., & Aarsnes, K. (2015). In-flight calibration of NOAA POES proton detectors — Derivation of the MEPED correction factors. *Journal of Geophysical Research: Space Physics*. Retrieved from http://dx.doi.org/10.1002/2015JA021388 doi: 10.1002/2015JA021388

Shprits, Y. Y., Drozdov, A. Y., Spasojevic, M., Kellerman, A. C., Usanova, M. E., Engebretson, M. J., ... others (2016). Wave-induced loss of ultra-relativistic electrons in the van allen radiation belts. *Nature communications*, *7*(1), 1–7.

Smirnov, A. G., Berrendorf, M., Shprits, Y. Y., Kronberg, E. A., Allison, H. J., Aseev, N. A., ... Effenberger, F. (2020). Medium energy electron flux in earth's outer radiation belt (merlin): A machine learning model. *Space Weather*, *18*(11), e2020SW002532. Retrieved from https://agupubs.onlinelibrary.wiley.com/doi/abs/10.1029/2020SW002532 (e2020SW002532 10.1029/2020SW002532) doi: 10.1029/2020SW002532

Summers, D., & Thorne, R. M. (2003). Relativistic electron pitch-angle scattering by electromagnetic ion cyclotron waves during geomagnetic storms. *Journal of Geophysical Research: Space Physics*, *108*(A4). Retrieved from http://dx.doi.org/10.1029/2002JA009489 doi: 10.1029/2002JA009489

Troitskaya, V. A. (1961, 1). Pulsation of the Earth's electromagnetic field with periods of 1 to 15 seconds and their connection with phenomena in the high atmosphere. *Journal of Geophysical Research*, *66*(1), 5–18. doi: 10.1029/JZ066i001p00005

Tsyganenko, N., & Sitnov, M. (2005). Modeling the dynamics of the inner magnetosphere during strong geomagnetic storms. *Journal of Geophysical Research: Space Physics*, *110*(A3).

Usanova, M. E., Drozdov, A., Orlova, K., Mann, I. R., Shprits, Y., Robertson, M. T., ... Wygant, J. (2014). Effect of EMIC waves on relativistic and ultrarelativistic electron populations: Ground-based and Van Allen Probes observations. *Geophysical Research Letters*, *41*(5), 1375–1381. Retrieved from http://dx.doi.org/10.1002/2013GL059024 doi: 10.1002/2013GL059024

Woodger, L. A., Halford, A. J., Millan, R. M., McCarthy, M. P., Smith, D. M., Bowers, G. S., ... Liang, X. (2015). A summary of the BARREL campaigns: Technique for studying electron precipitation. *Journal of Geophysical Research: Space Physics*, *120*(6), 4922–4935. Retrieved from http://dx.doi.org/10.1002/2014JA020874 doi: 10.1002/2014JA020874

Woodger, L. A., Millan, R. M., Li, Z., & Sample, J. G. (2018). Impact of background magnetic field for emic wave-driven electron precipitation. *Journal of Geophysical Research: Space Physics*, *123*(10), 8518-8532. Retrieved from https://agupubs.onlinelibrary.wiley.com/doi/abs/10.1029/2018JA025315 doi: https://doi.org/10.1029/2018JA025315

Yando, K., Millan, R. M., Green, J. C., & Evans, D. S. (2011). A Monte Carlo simulation of the NOAA POES Medium Energy Proton and Electron Detector instrument. *Journal of Geophysical Research: Space Physics*, *116*(A10). Retrieved from http://dx.doi.org/10.1029/2011JA016671 doi: 10.1029/2011JA016671

Yu, Y., Koller, J., Zaharia, S., & Jordanova, V. (2012). L* neural networks from different magnetic field models and their applicability. *Space Weather*, *10*(2). Retrieved from https://agupubs.onlinelibrary.wiley.com/doi/abs/10.1029/2011SW000743 doi: https://doi.org/10.1029/2011SW000743

Zhang, X.-J., Mourenas, D., Artemyev, A. V., Angelopoulos, V., & Sauvaud, J.-A. (2019). Precipitation of mev and sub-mev electrons due to combined effects of emic and ulf waves. *Journal of Geophysical Research: Space Physics*, *124*(10), 7923-7935. Retrieved from https://agupubs.onlinelibrary.wiley.com/doi/abs/10.1029/2019JA026566 doi: https://doi.org/10.1029/2019JA026566

Ødegaard, L.-K. G., Tyssøy, H. N., Sandanger, M. I. J., Stadsnes, J., & Søraas, F. (2016). Space Weather impact on the degradation of NOAA POES MEPED proton detectors. *J. Space Weather Space Clim.*, *6*, A26. Retrieved from https://doi.org/10.1051/swsc/2016020 doi: 10.1051/swsc/2016020

Figure 1.

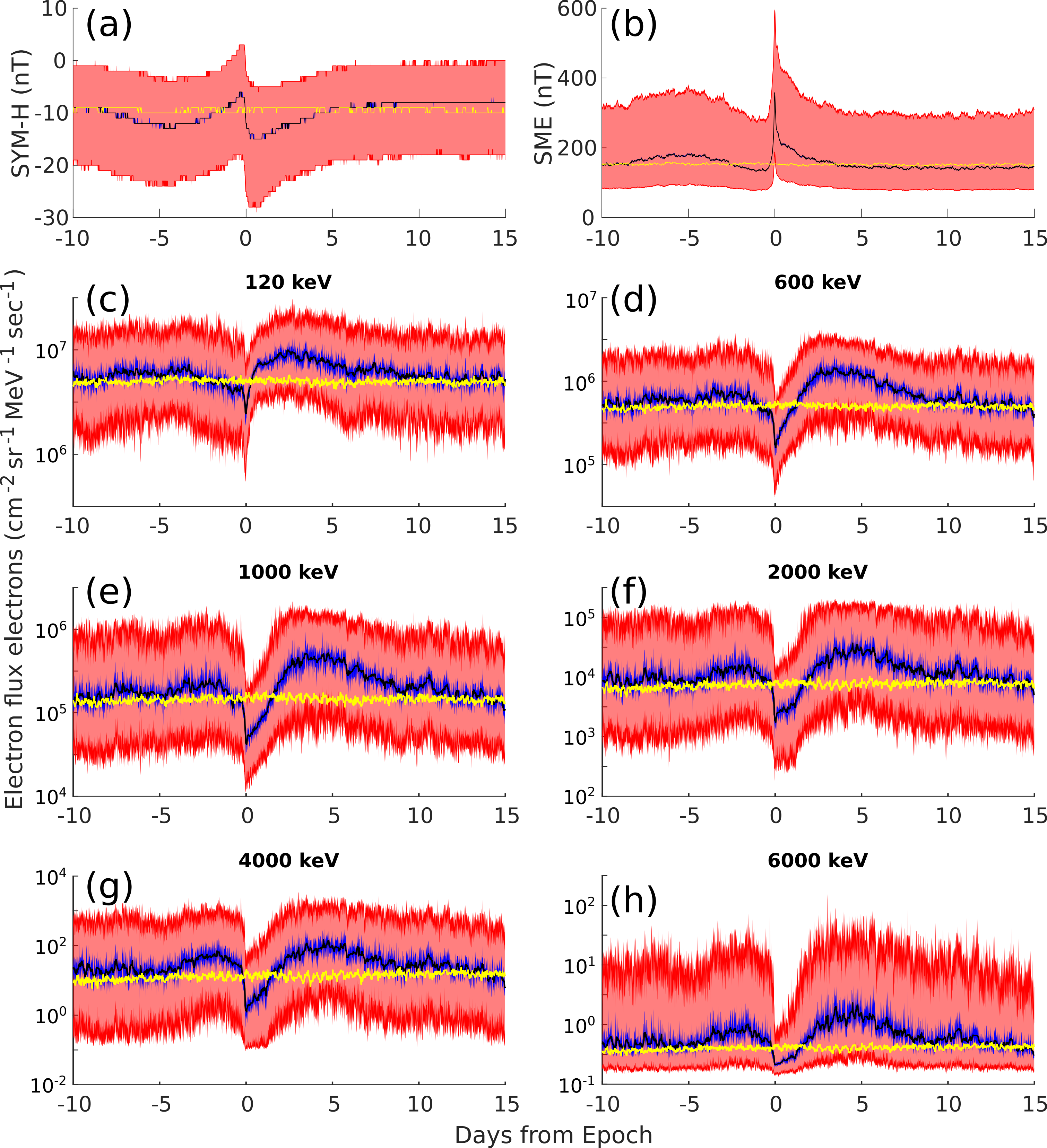

(a)
SYM-H (nT)
(b)
SME (nT)
120 keV
(c)
600 keV
(d)
1000 keV
(e)
2000 keV
(f)
4000 keV
(g)
6000 keV
(h)
Electron flux electrons (cm^{-2} sr^{-1} MeV^{-1} sec^{-1})
Days from Epoch

Figure 2.

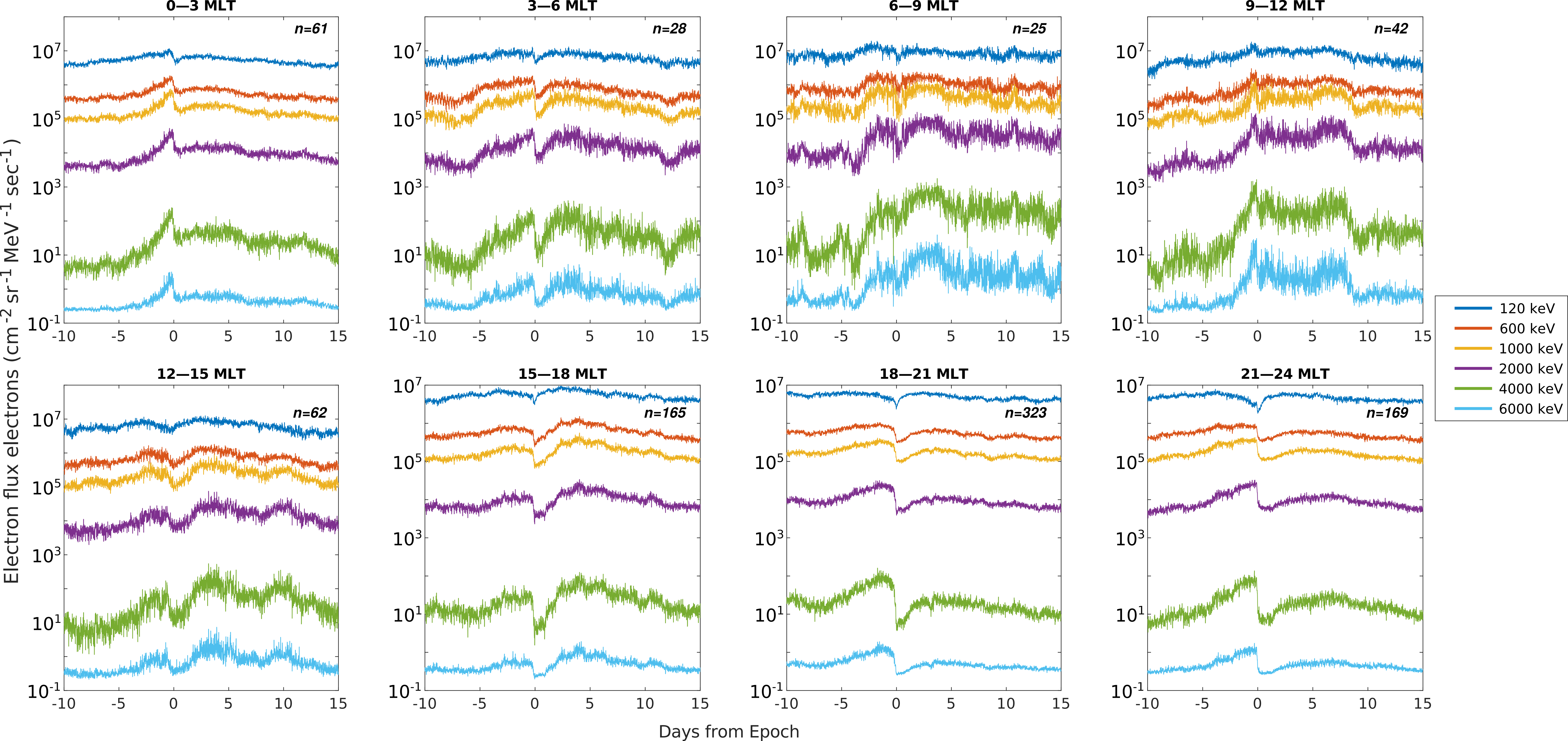

0—3 MLT
n=61
3—6 MLT
n=28
6—9 MLT
n=25
9—12 MLT
n=42
12—15 MLT
n=62
15—18 MLT
n=165
18—21 MLT
n=323
21—24 MLT
n=169
Electron flux electrons (cm^{-2} sr^{-1} MeV^{-1} sec^{-1})
Days from Epoch
120 keV
600 keV
1000 keV
2000 keV
4000 keV
6000 keV